

Frequency-stabilization to 6×10^{-16} via spectral-hole burning

Michael J. Thorpe,^{1*} Lars Rippe,² Tara M. Fortier¹, Matthew S. Kirchner¹,
and Till Rosenband¹

¹National Institute of Standards and Technology,
325 Broadway St., Boulder, CO 80304, USA

²Department of Physics, Atomic Physics, Lund University,
Professorsgata 1, 223 63 Lund, Sweden

*Address correspondence to; E-mail: mthorpe@nist.gov.

October 23, 2018

We demonstrate two-stage laser stabilization based on a combination of Fabry-Pérot and spectral-hole burning techniques. The laser is first pre-stabilized by the Fabry-Pérot cavity to a fractional-frequency stability of $\sigma_y(\tau) < 10^{-13}$. A pattern of spectral holes written in the absorption spectrum of $\text{Eu}^{3+}:\text{Y}_2\text{SiO}_5$ serves to further stabilize the laser to $\sigma_y(\tau) = 6 \times 10^{-16}$ for $2 \text{ s} \leq \tau \leq 8 \text{ s}$. Measurements characterizing the frequency sensitivity of $\text{Eu}^{3+}:\text{Y}_2\text{SiO}_5$ spectral holes to environmental perturbations suggest that they can be more frequency-stable than Fabry-Pérot cavities.

1 Introduction

Frequency-stable laser-local-oscillators (LLOs) are limiting components of the new generation of optical atomic clocks. Quieter LLOs would allow optical clocks to run more stably, yielding faster comparison measurements among different clocks, for more precise gravitational measurements and tests of fundamental physics [1, 2, 3]. Quieter LLOs may also yield lower-phase-noise microwave oscillators by frequency-division via femtosecond laser frequency combs [4, 5].

State-of-the-art LLOs are based on lasers that are tightly locked to high-finesse Fabry-Pérot (FP) cavities constructed from low thermal expansion glass. The Pound-Drever-Hall (PDH)

locking technique [6] provides sufficient signal-to-noise ratio (SNR) to lock the laser to the FP cavity, such that the laser’s fractional frequency stability beyond $\tau = 0.1$ s is limited only by the fractional optical-length stability of the cavity. Over the past decade, the stability of these systems has improved from 3×10^{-16} for durations of 1 to 100 seconds [7], to a recent demonstration of 2×10^{-16} for durations of 2 to 10 seconds [8]. During this time, practical concerns such as vibration-sensitivity have been addressed [9, 10, 11, 12], but lowering the noise floor has proved challenging. Numata *et al.* identified thermo-mechanical noise as the fundamental physical effect that limits the length stability of such cavities [13], and this insight was confirmed experimentally [14]. Thermo-mechanical noise may be reduced by using longer cavities [8], by choosing cavity, mirror and mirror-coating materials with a reduced mechanical loss tangent, by operating the cavity at lower temperatures or by using larger-diameter optical modes. However, all of these approaches present significant technical difficulties.

Spectral-hole burning in cryogenically cooled crystals has been demonstrated as an alternative to FP cavities for laser-stabilization [15, 16, 17, 18]. In such systems, the instantaneous laser frequency excursions are compared to the spectral memory stored in a crystal, and an error signal is derived to stabilize the laser. A fractional-frequency stability of $\sigma_y(\tau) = 3 \times 10^{-14}$ for $\tau = 10$ ms has been demonstrated [16], but at longer times the instability was significantly higher due to the transient nature of holes in $\text{Tm}^{3+}:\text{Y}_2\text{Al}_5\text{O}_{12}$ and high photon fluxes that acted to degrade the spectral memory. Although initial demonstrations of spectral-hole-burning laser locks did not reach the stability of FP-cavities, we expect the fundamental thermomechanical noise limit to be lower, because spectral holes are atomic frequency references that are perturbed only weakly through coupling to the crystal host. Hence, the spectral-hole reference frequency is largely decoupled from the crystal’s thermomechanical noise.

Several properties of $\text{Eu}^{3+}:\text{Y}_2\text{SiO}_5$ have motivated high-resolution spectroscopy of spectral holes. Both the ground (7F_0) and excited (5D_0) states of the Eu^{3+} laser stabilization transition have small magnetic moments, making them insensitive to magnetic field fluctuations [19]. The 5D_0 excited state has a lifetime of 1.9 ms and photon echo measurements indicate linewidths as low as 122 Hz for the ${}^7F_0 \rightarrow {}^5D_0$ transition [20, 21]. When Eu^{3+} is doped into the Y_2SiO_5 crystal, each ion experiences a slightly different crystal field that causes a different Stark shift for each absorber. As a result, the $\text{Eu}^{3+}:\text{Y}_2\text{SiO}_5$ absorption spectrum is inhomogeneously broadened to a width that depends linearly on the doping concentration [22, 23]. For the present work, we used a doping of 0.5% Eu^{3+} , corresponding to an inhomogeneous linewidth of 10 GHz that, in principle, can contain nearly 10^8 resolvable spectral holes. $\text{Eu}^{3+}:\text{Y}_2\text{SiO}_5$ spectral holes can also be long-lived. At $T = 2.0$ K, a lifetime of 20 days has been measured [22]. However, the lifetime depends strongly on temperature. For our nominal operating temperature ($T = 4.5$ K) the lifetime is more than 1 day, but the spectral holes last only 1 s at 15 K. Therefore, a spectral-hole pattern can be used for long-term laser stabilization at $T \leq 4.5$ K, and can be easily erased if the crystal temperature is temporarily increased.

Here we describe a two-stage laser-stabilization system (Fig. 1), where a FP cavity first stabilizes the laser frequency to $\sigma_y(\tau) \approx 10^{-14}$ (0.1 s $< \tau < 10$ s). The pre-stabilized laser is then modulated to address 10^{15} atomic absorbers within a 5 mm length and 1 cm diameter

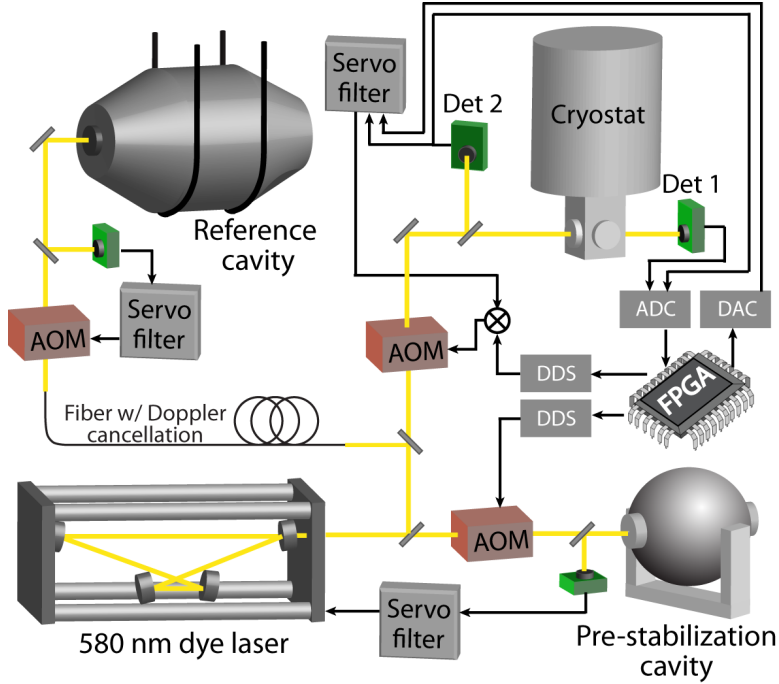


Figure 1: The $\text{Eu}^{3+}:\text{Y}_2\text{SiO}_5$ spectroscopy and laser stabilization experimental setup. Spectroscopy is performed with a pre-stabilized 580 nm dye laser that illuminates a $\text{Eu}^{3+}:\text{Y}_2\text{SiO}_5$ crystal housed in an optical flow cryostat. A field-programmable gate array (FPGA) with an embedded microprocessor controls the details of the spectroscopy including laser frequency, light intensity and pulse durations. The frequencies of spectral holes can be compared against the frequency of the pre-stabilization cavity, or against a reference cavity that typically stabilizes the Al^+ clock laser.

$\text{Eu}^{3+}:\text{Y}_2\text{SiO}_5$ crystal. This servo simultaneously writes and stabilizes the laser to a pattern of spectral holes in the $\text{Eu}^{3+}:\text{Y}_2\text{SiO}_5$ absorption spectrum. By using a pre-stabilized laser and many spectral holes we derive an error signal for laser stabilization while reducing perturbations to the spectral memory. Here we demonstrate the use of 10 to 100 spectral holes to stabilize a 580 nm laser to $\sigma_y(\tau) = 6 \times 10^{-16}$ for $2 \text{ s} < \tau < 8 \text{ s}$. We also report several properties of $\text{Eu}^{3+}:\text{Y}_2\text{SiO}_5$ that make this material a promising candidate for achieving higher laser stability than is currently available via optical cavities.

2 Results

The absorption spectrum for the ${}^7\text{F}_0 \rightarrow {}^5\text{D}_0$ transition in 0.5% doped $\text{Eu}^{3+}:\text{Y}_2\text{SiO}_5$ at $T = 4.5 \text{ K}$ is shown in figure 2(a). The two resolved peaks at vacuum wavelengths of 580.0390 nm and 580.2110 nm result from two different locations within the Y_2SiO_5 crystal unit cell where

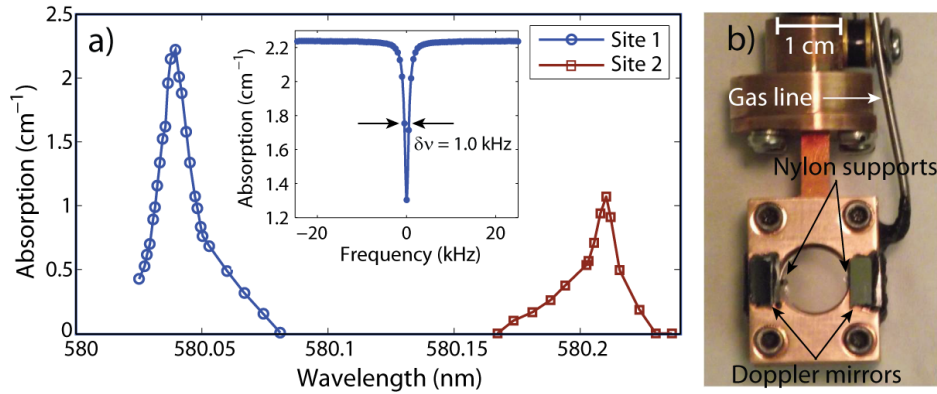


Figure 2: a) The absorption spectrum of the ${}^7F_0 \rightarrow {}^5D_0$ transition in 0.5% doped $\text{Eu}^{3+}:\text{Y}_2\text{SiO}_5$ at $T = 4.5$ K. The two inhomogeneously broadened absorption features ‘sites 1 & 2’ result from the two different positions within the Y_2SiO_5 unit cell where Eu^{3+} can substitute for Y^{3+} . The inset shows a single spectral hole written at 580.0390 nm and $T = 4.5$ K with a burn time of 100 ms and a laser intensity of $35 \mu\text{W}/\text{cm}^2$. This hole was measured with 2 ms probe pulses, each separated by 500 Hz (SNR = 1500). b) A picture of the sealed chamber that provides a controlled pressure environment and acceleration insensitive mounting for the $\text{Eu}^{3+}:\text{Y}_2\text{SiO}_5$ crystal.

Eu^{3+} can substitute for Y^{3+} . These features are referred to as sites 1 and 2, respectively. The inset in figure 2(a) shows a single spectral hole with a linewidth of 1.0 kHz, a 40% contrast and an SNR of 1500, written at 580.0390 nm and $T = 4.5$ K. Although photon-echo measurements suggest that $\text{Eu}^{3+}:\text{Y}_2\text{SiO}_5$ spectral holes as narrow as 100 Hz are possible [21], so far we have not observed linewidths narrower than 500 Hz. This broader linewidth is partially due to phonon scattering that contributes 300 Hz to the homogeneous linewidth at $T = 4.5$ K [22]. Further broadening may be caused by vibrations or fluctuations in electric or magnetic fields in our cryostat, which can be improved in future systems. We used two protocols for writing and detecting spectral holes. For characterizing the sensitivity to environmental perturbations we wrote the holes at a relatively high intensity ($35 \mu\text{W}/\text{cm}^2$ to $140 \mu\text{W}/\text{cm}^2$) for durations of 10 ms to 200 ms, and detected the holes at lower intensities ($3 \mu\text{W}/\text{cm}^2$) with shorter pulse durations (1 ms). For laser stabilization we wrote and detected the pattern with the low intensity ($3 \mu\text{W}/\text{cm}^2$) and short duration (1 ms) pulses.

The $\text{Eu}^{3+}:\text{Y}_2\text{SiO}_5$ crystal is housed in an optical flow cryostat that provides the ability to continuously vary the crystal temperature from 2.0 K to 300 K (Fig. 1). Inside the cryostat, the crystal is enclosed in a second sealed chamber that is filled with helium gas, so that the pressure and temperature environment can be controlled independently (Fig. 2(b)). A gas line leads from the sealed chamber to a manifold outside the cryostat where the pressure is controlled and monitored. Figure 3 shows the pressure and temperature sensitivity of the spectral-hole frequency. The pressure sensitivities, $\alpha_1 = -211.4(4)$ Hz/Pa for site 1 and $\alpha_2 = -52.0(7)$ Hz/Pa

for site 2, are shown in figure 3(a). By combining the pressure sensitivity with the bulk modulus of Y_2SiO_5 (135 GPa), we calculate the sensitivity of spectral holes to changes in the volume of the crystal ($\delta f/f = 0.055 \times \delta V/V$ for site 1 and $\delta f/f = 0.014 \times \delta V/V$ for site 2). Compared to FP cavities where $\delta f/f = 0.33 \delta V/V$ and the typical bulk modulus is 34 GPa [24], spectral holes have significant isolation from mechanical instability that not only makes them less sensitive to accelerations, but also reduces their susceptibility to thermal noise.

Measurements of the temperature sensitivity for sites 1 and 2 are shown in figures 3(b) & 3(c) respectively. The data show the temperature sensitivities κ_i for sites ($i \in \{1, 2\}$) in the absence of a background gas ($P = 0$ Pa). Site 1 displays a lower temperature sensitivity than site 2, and an anomalous backward bending of the curve at 7.5 K. These curves provide a high-resolution extension of data presented by Könz *et al.* [22]. When the sealed chamber is filled with helium gas, the pressure and temperature of the gas are related through the ideal gas law. Furthermore, since the pressure sensitivity has a negative slope, and the temperature sensitivity has a positive slope (for $2.0 \text{ K} < T < 7.5 \text{ K}$) certain combinations of pressure and temperature lead to a vanishing first-order term of the temperature sensitivity. This effect is illustrated in figures 3(b) & 3(c). Because the gas manifold is outside the cryostat, at room temperature, the gas behaves as a two-reservoir system. The equation of state for this system (see Methods section) can be combined with the pressure sensitivity $\alpha_i \Delta P$ and the zero-pressure temperature sensitivity $\kappa_i(T_c)$ functions for each site to determine the spectral-hole temperature sensitivity in the presence of helium gas:

$$f_i(P, T_c) = \kappa_i(T_c) + \alpha_i P(T_c). \quad (1)$$

Here f_i is the spectral-hole frequency, $P(T_c)$ is the equation of state and T_c is the temperature of the crystal inside the cryostat. A fit to the measured data determines the ratio of the cryogenic to room temperature gas volumes for the current system, $V_c/V_r = 0.022(3)$. This ratio is important because it determines how strongly temperature and pressure fluctuations in the gas manifold (outside the cryostat) will affect the temperature and pressure of the cryogenic gas volume. The temperature-insensitive points for spectral holes have some advantages over the analogous ‘zero-crossing temperature’ of the coefficient of thermal expansion for ultra-low expansion glass (ULE) cavities. First, the temperature of the insensitive point for spectral holes can be tuned by changing the pressure of helium gas in the sealed chamber. Second, the spectral holes exhibit reduced temperature sensitivity compared to ULE. For ULE, the quadratic temperature sensitivity is 720 kHz/K² for a cavity operating at 580 nm [24]. The values for $\text{Eu}^{3+}:\text{Y}_2\text{SiO}_5$ spectral-holes are 16 kHz/K² for site 1 and 114 kHz/K² for site 2.

A pattern of spectral holes, simultaneously written and used for laser stabilization, is shown in figure 4(a). For details about the writing and probing of the spectral-hole pattern, refer to the Methods section. During laser stabilization, the pressure and temperature of the crystal environment are held at an insensitive point. At the same time, a Doppler measurement cancels frequency shifts in the spectral-hole pattern due to the motion of the crystal [25]. This measurement is made with a Michelson interferometer where one arm of the interferometer is formed by a mirror attached to the crystal chamber (see Fig. 2(b)). Figure 4(b) shows the

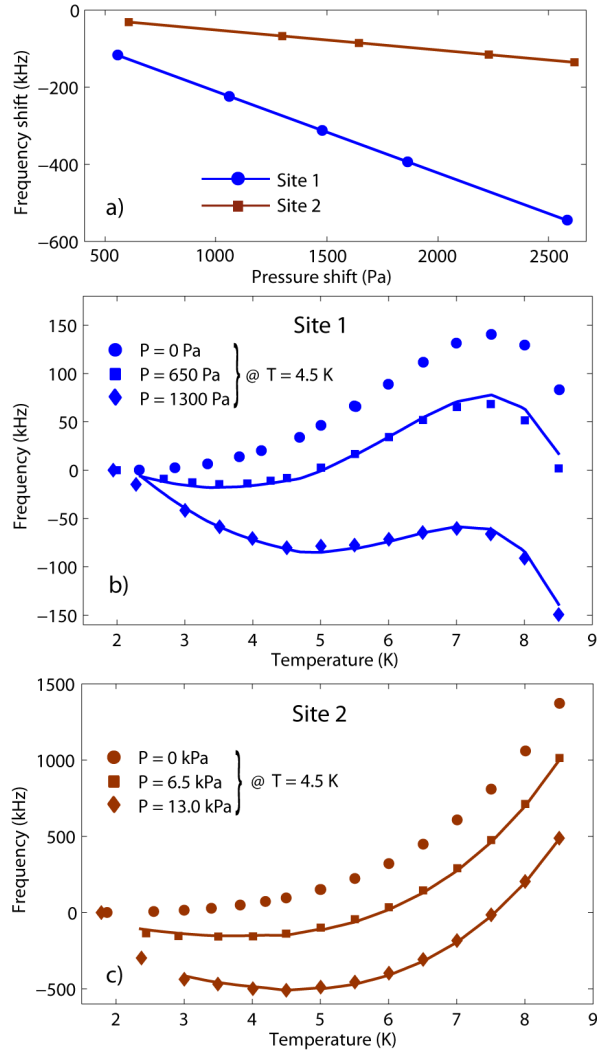


Figure 3: The pressure and temperature sensitivity of the spectral-hole frequency for sites 1 and 2. a) Pressure sensitivity is $\alpha_1 = -211.4(4)$ Hz/Pa for holes at site 1 and $\alpha_2 = -52.0(7)$ Hz/Pa at site 2. b) & c) The temperature sensitivities for holes at sites 1 & 2 are given by the $P = 0$ Pa data (circles). In a sealed chamber, the gas pressure and temperature are linked by the ideal gas law, and the pressure and temperature sensitivities both contribute to the frequency of the spectral hole. At certain combinations of P and T for each site, the frequency becomes first-order insensitive to the temperature of its environment. The solid lines through the $P \neq 0$ data are expected frequency shifts given the measured pressure and temperature sensitivities and the best fit volume ratio (see text).

frequency spectrum of the spectral-hole-stabilized laser with and without Doppler cancellation. Two prominent resonances in the crystal motion appear at 14.5 Hz and 33 Hz, corresponding

to RMS frequency shifts of 12.1 Hz and 4.3 Hz respectively. When Doppler cancellation is implemented, these shifts are reduced, improving the frequency stability of the hole pattern. The residual frequency shift of 0.25 Hz amplitude (RMS) due to the 14.5 Hz motion provides an estimate of the acceleration sensitivity of the spectral-hole pattern of $7 \times 10^{-12} \text{ g}^{-1}$ ($1 \text{ g} = 9.8 \text{ m/s}^2$), which is an order of magnitude below the lowest passive acceleration-sensitivity of FP cavities [8, 11, 26]. As in FP cavities, the acceleration sensitivity depends on the mounting configuration, and further improvements are possible. For the present work, the crystal is supported on two 0.8 mm thick and 2.5 mm wide nylon tabs (Fig. 2(b)). The support points are

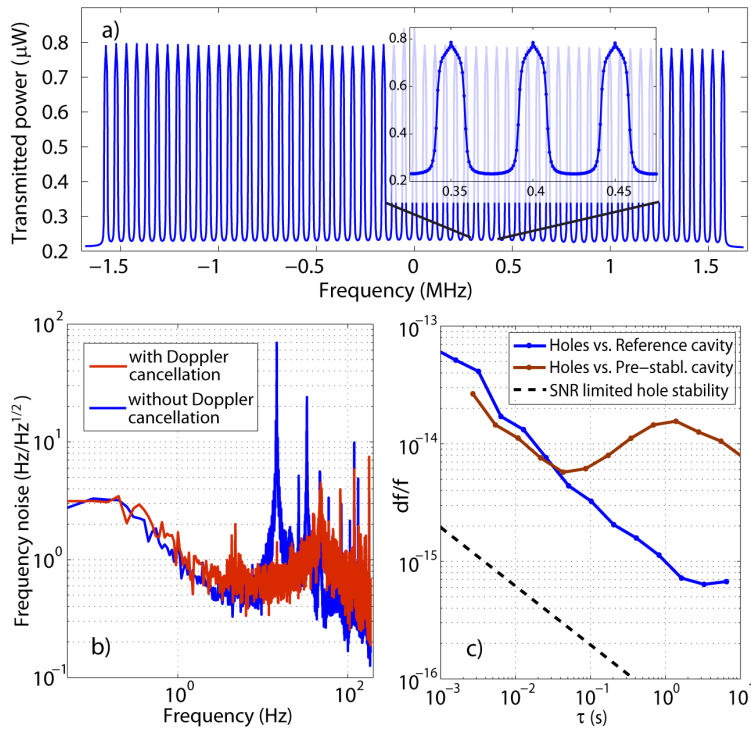


Figure 4: a) A pattern of 61 spectral holes spaced by 50 kHz for laser stabilization. The inset shows three of the holes in higher resolution. b) Laser frequency noise spectra of the spectral-hole laser lock with and without Doppler cancellation of the crystal motion (30 mHz resolution bandwidth). The motional resonance at 14.5 Hz sets an upper limit on the spectral-hole acceleration sensitivity of $7 \times 10^{-12} \text{ g}^{-1}$. c) Allan deviation traces of frequency comparisons between the pre-stabilization cavity, the reference cavity, and the spectral-hole pattern. The pre-stabilized laser is made artificially noisy, $\sigma_y(\tau) > 10^{-14}$ (red trace), and is used to write and lock to a pattern a spectral holes. The spectral-hole lock is then compared to the frequency of a reference cavity that has a noise floor of $\sigma_y(\tau) \approx 5 \times 10^{-16}$ (blue trace). The black dashed line is the expected short-term stability based on the spectral-hole linewidth and the SNR of the absorption measurements.

near the vertical center of the crystal such that the frequency of spectral holes are nominally insensitive to accelerations [9].

To determine the frequency stability of the spectral-hole laser lock, we independently locked the 580 nm laser to a reference cavity that is typically used to stabilize the clock laser for the $^{27}\text{Al}^+$ optical clock [27]. To ensure that the write/probe laser was locked tightly to the spectral-hole pattern, we injected noise into the pre-stabilization servo, thereby degrading the laser stability to $\sigma_y \approx 10^{-14}$. Figure 4(c) shows the write/probe laser stability and the frequency comparison between the reference cavity and the spectral-hole laser lock with the linear frequency drift subtracted. The reference cavity has a noise floor of $\sigma_y(\tau) \approx 5 \times 10^{-16}$, and a typical drift rate of 0.1 Hz/s. During the comparison measurements, we observed relative drifts between the spectral-hole pattern and the reference cavity that varied between 0.1 Hz/s to 0.5 Hz/s. A noise floor of $\sigma_y = 6.5 \times 10^{-16}$ was observed in the comparison. So far, we have not observed signal-to-noise-ratio-limited short-term stability of the spectral-hole laser lock (see Fig. 4(c)). We expect that this is due to a combination of pressure fluctuations of the gas reservoir, vibrations in cryostat, and Dick-effect noise from the write/probe laser due to the 90% duty cycle of our probe pulses. Each of these sources of instability must be addressed to achieve SNR-limited performance.

3 Discussion

Our initial attempts at laser stabilization have already demonstrated performance that is competitive with the best FP cavities on short time scales. Further improvements are expected from the use of two probe beams that enable interleaved measurements of the hole pattern to eliminate Dick effect noise. To reach a stability of $\sigma_y(\tau) = 3 \times 10^{-17} / \sqrt{\tau}$ will require $\Delta P < 67 \mu\text{Pa}$ and $\Delta a < 4 \mu\text{g}$ at 1 s of averaging time, and can be achieved through better engineering of the cryogenic environment. Magnetic field sensitivity measurements indicate that a modest control of the magnetic field $\Delta B < 10^{-5} \text{ T}$ will be required. Finally, due to the pressure and temperature cancellation at the site 1 insensitive point, an overall temperature stability of $\Delta T < 1.4 \text{ mK}$ is sufficient, but temperature gradients must also be minimized. This technique for achieving low temperature sensitivity may be useful for other proposed frequency references based on solids such as Thorium-doped crystals [28, 29].

At longer time scales, frequency comparison measurements are currently limited by the lifetime of the spectral-hole pattern. This limitation needs to be addressed if spectral-hole burning laser stabilization is to become useful for most LLO applications. One approach for dealing with this problem is to write a self-regenerating pattern that eventually achieves a quasi-steady state. Such a spectral-hole pattern is possible if the pattern of holes is wide enough to encompass all of the Eu^{3+} hyperfine ground states, and the hole spacing is small enough to prevent population buildup between adjacent spectral holes. Stabilization to such a steady-state pattern must also compensate for the side-holes and anti-holes that accompany each spectral feature [20].

If the technical sources of frequency noise can be made sufficiently small, the stability

of $\text{Eu}^{3+}:\text{Y}_2\text{SiO}_5$ spectral holes will be determined by thermal noise. Our measurements of the pressure sensitivity provide some insight into this fundamental limit. If we assume an isotropic crystal geometry and a conservative mechanical loss angle for $\text{Eu}^{3+}:\text{Y}_2\text{SiO}_5$ ($\phi = 10^{-3}$) then thermal noise for a crystal of the size used in the present work implies a fractional-frequency instability below 3×10^{-17} [13]. However, many crystalline materials exhibit reduced mechanical loss at cryogenic temperatures, therefore the mechanical loss angle at 4.5 K may be smaller ($\phi \approx 10^{-5}$) leading to a thermal noise floor that is an order of magnitude lower. Nevertheless, Y_2SiO_5 has low crystal symmetry, and a full anisotropic treatment of its thermo-mechanical properties is required to make accurate estimates of the thermal noise floor [30], as well as to engineer optimal strategies for mounting these crystals to minimize environmental sensitivity.

During the past decade, the frequency-stabilities of LLOs based on either FP cavities or spectral-hole burning have improved by 30%, and new optical clocks have a substantial need for further improvements. A combination of the two laser-stabilization approaches has the potential to yield order-of-magnitude stability gains due to the low sensitivity of $\text{Eu}^{3+}:\text{Y}_2\text{SiO}_5$ spectral holes to environmental perturbations and internal noise. Such gains could benefit a wide range of LLO applications including the realization of atomic time, gravitational measurements for geodesy, radar and communications applications and very long baseline interferometry.

4 Methods

The experimental setup for high-resolution spectroscopy of $\text{Eu}^{3+}:\text{Y}_2\text{SiO}_5$ spectral holes is shown in Fig. 1. The output of a 580 nm dye laser is split into three beam-lines that provide pre-stabilization of the laser frequency, frequency comparisons with a reference cavity, and a write/probe beam for $\text{Eu}^{3+}:\text{Y}_2\text{SiO}_5$ spectroscopy. The laser is locked to the pre-stabilization cavity using the PDH scheme. With optimal locking, the laser can achieve a stability of $\sigma_y(\tau) = 1.2 \times 10^{-15}$ ($0.5 \text{ s} < \tau < 12 \text{ s}$) [26]. For spectral-hole laser locking experiments we intentionally reduce the stability of the write/probe laser ($\sigma_y(\tau) > 10^{-14}$ for $0.3 \text{ s} < \tau < 6 \text{ s}$) to clearly demonstrate the stability of the spectral holes. An acousto-optic modulator (AOM) is placed before the cavity, enabling laser frequency adjustments of the ‘reference cavity’ and ‘write/probe’ beam-lines that are independent of the pre-stabilization cavity lock.

For temperatures above 4.2 K, the crystal temperature is controlled by a servo that heats helium vapor surrounding the sealed chamber. For temperatures below 4.2 K, the heater is turned off and a scroll pump and a pressure regulator are used to lower the pressure, and hence the temperature, of the helium vapor. In the range from 2.0 K to 10.0 K the temperature can be controlled to within 1 mK. The sealed chamber is filled with helium gas by a 0.9 mm inner diameter tube that extends from the chamber inside the cryostat to the room temperature gas manifold. A capacitive pressure gauge located on the room temperature gas manifold is used to monitor the pressure inside the sealed chamber. The pressure and temperature of this system

are related by

$$P = \frac{k_B C T_c}{1 + \frac{T_c V_r}{T_r V_c}}, \quad (2)$$

where P is the pressure of the system, k_B is the Boltzmann constant, T_r (T_c) correspond to the room (cryostat) temperature, V_r (V_c) are the room temperature (cryogenic) gas volumes and C is the total number of helium atoms divided by V_c .

$\text{Eu}^{3+}:\text{Y}_2\text{SiO}_5$ spectroscopy is performed by measuring the frequency-dependent absorption of light transmitted through the $\text{Eu}^{3+}:\text{Y}_2\text{SiO}_5$ crystal. For the current work, the crystal was illuminated by a 6 mm diameter beam. The intensity, frequency, and duration of the illumination are controlled by a microprocessor that is embedded in a field programmable gate array (FPGA). The FPGA instructs a digital to analog converter (DAC) to output voltage pulses to an intensity servo to control the optical power and pulse duration. Prior to each pulse, the FPGA sets the frequency of a direct digital synthesizer (DDS) that drives the broadband AOM located before the cryostat. In the current setup, the frequency of the incident beam can be tuned over 600 MHz of bandwidth, and the beam intensity can be set to values between $0.1 \mu\text{W}/\text{cm}^2$ and $200 \mu\text{W}/\text{cm}^2$. The incident and transmitted beams, detected by ‘Det 1’ and ‘Det 2’ and digitized by an analog-to-digital converter (ADC), are used to calculate the absorption for each experiment.

For laser stabilization experiments, the embedded microprocessor controls the process for simultaneously writing and probing the spectral-hole pattern. Experimental parameters such as the number of holes, hole spacing, center frequency of the pattern, servo gains, pulse duration and pulse power are adjustable by the user. To generate a spectral-hole pattern, a single hole is first burned with successive pulses until a target hole-depth (typically 30% contrast) is reached. Each time a hole reaches the target depth, the burning process for a new hole is initiated until the pattern contains the pre-specified number of holes. When holes exceed the target depth they are deemed ready for laser stabilization. During the burning process there are two categories of holes, those ready for stabilization and those still in the burning process. The servo interleaves burning pulses on unfinished holes with frequency stabilization measurements on sufficiently deep holes until all holes have exceeded the target depth. For each frequency measurement and burn operation, a random hole is selected from the corresponding group. This bootstrapping process establishes a regular pattern of spectral holes.

Frequency stabilization measurements are made by recording the absorption on both sides of a hole at roughly $2/3$ of the maximum depth. These measurements are subtracted, multiplied by the servo gain, and fed-back to the frequency of the AOM positioned before the pre-stabilization cavity. As the holes are continually measured, they become both deeper and wider. The frequency measurement data is used in a secondary feedback loop to track the width of each hole to ensure that servo measurements are always made at roughly $2/3$ of the hole depth. For each frequency measurement the hole is also burned at the center frequency until its contrast approaches 100% so that each hole retains a single-peaked shape. Once all holes reach full contrast, only frequency measurements are performed and the measurement duty cycle is 90%. Finally, a small amount of gain is used to adjust the laser probe frequency for each hole

to remove frequency errors that occur because the holes are written with a noisy laser.

To determine the stability of the pre-stabilization cavity and spectral-hole pattern laser locks, frequency comparisons are made with a reference cavity. Light from the dye laser is delivered to the reference cavity over a Doppler-noise-canceled fiber. The laser is locked to the reference cavity with a PDH error signal is fed-back to an AOM positioned before the cavity. When locked, the AOM drive frequency provides a measure of the frequency difference between the reference cavity and the pre-stabilization cavity (if the spectral-hole laser lock is inactive) or the spectral-hole laser lock when it is active.

5 Acknowledgements

M. J. Thorpe acknowledges support from the National Research Council. The authors thank R. L. Cone, J. C. Bergquist, J. Ye, J. L. Hall and D. J. Wineland for useful discussions, and D. R. Leibbrandt and J. A. Sherman for help with manuscript preparation. This work is supported by DARPA and ONR and is not subject to U.S. copyright.

6 Author Contributions

M.J.T, T.R. and L.R. designed the experiments. M.J.T., T.M.F. and M.S.K. performed the experiments. M.J.T. and T.R. conducted the data analysis. M.J.T., T.R., L.R. and M.S.K. wrote the manuscript.

References

- [1] T. Rosenband, *et al.*, *Science* **28**, 1808-1812 (2008).
- [2] S. Blatt, *et al.*, *Phys. Rev. Lett.* **100**, 140801-1-4 (2008).
- [3] C. W. Chou, D. B. Hume, T. Rosenband, D. J. Wineland, *Science* **329**, 1630 (2010).
- [4] A. Bartels, S. A. Diddams, C. W. Oates, G. Wilpers, J. C. Bergquist, W. H. Oskay, L. Hollberg, *Opt. Lett.* **30**, 667-669 (2005).
- [5] T. M. Fortier, *et al.*, *arXiv:1101.3616v2* (2011).
- [6] R. W. P. Drever, J. L. Hall, F. V. Kowalski, J. Hough, G. M. Ford, A. J. Munley, H. Ward, *App. Phys. B* **31**, 97-105 (1983).
- [7] B. C. Young, F. C. Cruz, W. M. Itano, J. C. Bergquist, *Phys. Rev. Lett.* **82**, 3799-3802 (1999).

- [8] Y. Y. Jiang, A. D. Ludlow N. D. Lemke, R. W. Fox, J. A. Sherman, L.-S. Ma, C. W. Oats, *Nat. Photonics* **5**, 158-161 (2011).
- [9] M. Notcutt, L. S. Ma, J. Ye, J. L. Hall, *Opt. Lett.* **30**, 1815-1817 (2005).
- [10] T. Nazarova, F. Riehle, U. Sterr, *Appl. Phys. B* **83**, 531-536 (2006).
- [11] S. A. Webster, M. Oxborrow, P. Gill, *Phys. Rev. A* **75**, 011801-1-6 (2007).
- [12] M. J. Thorpe, D. R. Leibbrandt, T. M. Fortier, T. Rosenband, *Opt. Express* **18**, 18744-18751 (2010).
- [13] K. Numata, A. Kemery, J. Camp, *Phys. Rev. Lett.* **93**, 250602-1-4 (2004).
- [14] M. Notcutt, L.-S. Ma, A. D. Ludlow, S. A. Foreman, J. Ye, J. L. Hall, *Phys. Rev. A* **73**, 031804-1-4 (2006).
- [15] P. B. Sellin, S. N. M., J. L. Carlsten, R. L. Cone, *Opt. Lett.* **24**, 1038-1040 (1999).
- [16] N. M. Strickland, P. B. Sellin, Y. Sun, J. L. Carlsten, R. L. Cone, *Phys. Rev. B* **62**, 1473-1476 (2000).
- [17] T. Böttger, G. J. Pryde, R. L. Cone, *Opt. Lett.* **28**, 200-202 (2003).
- [18] B. Julsgaard, A. Walther, S. Kröll, L. Rippe, *Opt. Express* **15**, 11444-11465 (2007).
- [19] R. M. Shelby, R. M. Macfarlane, *Phys. Rev. Lett.* **47**, 1172-1175 (1981).
- [20] R. Yano, M. Mitsunaga, N. Uesugi, *Opt. Lett.* **16**, 1884-1886 (1991).
- [21] Equall, R. W., Y. Sun, R. L. Cone, R. M. Macfarlane, *Phys. Rev. Lett.* **72**, 2179-2182 (1994).
- [22] F. Könz, Y. Sun, C. W. Thiel, R. L. Cone, R. L. Equall, R. L. Htchenson, R. M. Macfarlane, *Phys. Rev. B* **68**, 085109-1-9 (2003).
- [23] M. J. Sellars, E. Fraval, J. J. Longdell, *J. Lumin.* **107**, 150-154 (2004).
- [24] Corning ule datasheet, <http://www.corning.com/docs/specialtymaterials/pisheets/ulebro91106.pdf>.
- [25] J. C. Bergquist, W. M. Itano, D. J. Wineland, *International School of Physics "Enrico Fermi"*, T. W. Hänsch, M. Inguscio, eds. (North-Holland, Amsterdam, 1994).
- [26] D. R. Leibbrandt, M. J. Thorpe, M. Notcutt, R. E. Drullinger, T. Rosenband, J. C. Bergquist, *Opt. Express* **19**, 3471-3482 (2011).
- [27] C. W. Chou, D. B. Hume, J. C. J. Koelemeij, D. J. Wineland, T. Rosenband, *Phys. Rev. Lett.* **104**, 070802-1-4 (2010).

- [28] E. Peik, Chr. Tamm, *Europhys. Lett.* **61**, 181-186 (2003).
- [29] W. G. Rellergert, D. DeMille, R. R. Greco, M. P. Hehlen, J. R. Torgerson, E. R. Hudson, *Phys. Rev. Lett.* **104**, 200802-1-4 (2010).
- [30] D. Heinert, *et al.*, *Journal of Physics: Conference Series* **228**, 012032-1-6 (2010).